Kinetic Analysis and Pyrolysis Behavior of Pine Needles by TG-FTIR and Py-GC/MS

Langui Xu,[a] Yujian Zhang,[a] Ziyong Wang,[b] Shurui Guo,[c] Yongxing Hao,[a] Yuguo Gao,[a] Min Xin,[d] Yi Ran,[e] Shuxun Li,[f] Rui Ji,[g] Hongmei Li,[g] Huixia Jiang,[h] Qingyan He,[c,h] and Ruyi Huang [a,d,e,*]

The pyrolysis performances and reaction kinetics of pine needles (PN) were investigated by integrating thermogravimetric analysis, Fourier transform infrared spectroscopy, and pyrolysis-gas chromatography/mass spectrometry. The average activation energy of PN was estimated to be 183.2 kJ/mol by Kissinger Akahira Sunose (KAS) and 183.8 kJ/mol by Flynn Wall Ozawa (FWO), respectively at heating rates of 10, 20, and 40 °C/min. The pyrolysis of PN was found to be more efficient at the lower heating rates, while increased heating rates promoted the reaction. Using the King-Kai (K-K) method, the activation energies of hemicellulose, cellulose, and lignin were calculated to be 156, 165, and 172 kJ/mol, respectively. The descending order of evolving gases and functional groups from PN was found to be CO_2, C=C, C=O, H_2O, CH_4, and CO. The main pyrolytic by-products identified were hydrocarbons, phenols, alcohols, ketones, and aldehydes. The determination of kinetic parameters provides fundamental information for predicting the rates at which chemical reactions occur. This study demonstrates the potential of PN as a suitable source for bioenergy.

DOI: 10.15376/biores.18.3.6412-6429

Keywords: Pine needle; Pyrolysis; Thermogravimetric analysis; TG–FTIR; Py–GC/MS

Contact information: a: School of Mechanical Engineering, North China University of Water Resources and Electric Power, Zhengzhou 450011, China; b: Henan ALST New Energy Technology Co. LTD, Zhengzhou 450001, China; c: College of Architecture and Environment, Sichuan University, Chengdu China, 610065; d: Rural Energy Development Center of Sichuan Province, Chengdu 610041, China; e: Biogas Institute of Ministry of Agriculture and Rural Affairs, Key Laboratory of Development and Application of Rural Renewable Energy, Ministry of Agriculture and Rural Affairs, Chengdu 610041, China; f: Sichuan Water Conservancy Vocational and Technical College, Chengdu 611830, China; g: Sichuan Agricultural Foreign Cooperation and Communication Center Chengdu 610041, China; h: Sichuan Research and Design Institute of Agricultural Machinery Chengdu 610066, China;
** Corresponding author: 28209443@qq.com*

INTRODUCTION

Biomass is an important alternative energy source due to its sustainability, carbon neutrality, and abundance (Wang *et al*. 2018; Huang *et al.* 2020). Through thermochemical conversion technology, energy recycling can be achieved (Ding *et al*. 2020). Forest residues have received extensive consideration as biofeedstock due to their wide geographical distribution, lower emissions released into the environment, and high biomass potential (Dhyani and Bhaskar 2018). Bioenergy is projected to rank as the fourth energy resource with a projected growth rate of 30%, following oil, coal, and natural gas (Yasmeen *et al*. 2022). Pine is a gymnosperm belonging to the Pinaceae family, and its leaves are needle-shaped, so it is named after "pine needle" (PN). There are rich PN resources in

China, with reserves of more than 100 million tons every year (Wang *et al*. 2020). Transforming PN into biofuel through pyrolysis and combustion can offer a comprehensive and sustainable solution to multiple issues. The accumulation of pine needles can pose challenges for local residents, including the risk of wildfires and environmental concerns.

During biomass combustion, the process typically starts with the pyrolysis stage. Pyrolysis is the thermal decomposition of biomass with limited oxygen supply. Under external heat, biomass undergoes several stages of pyrolysis, which can convert raw materials into bio-oil, bio-char, and pyrolytic gases (Gupta *et al*. 2019). For example, Fu *et al*. (2022) found that the pyrolysis of torrefied coffee grounds at 300 °C reduced the hydrocarbon proportion of bio-oils. According to Huang *et al.* (2020), the main pyrolytic products obtained from water hyacinth roots, stems, and leaves were phenols, furans, and nitrides. Pine trunks have been investigated in related literature, indicating their pyrolysis characteristics with the exclusion of their residues such as PN (Sun *et al*. 2017; Xu *et al*. 2020). The pyrolysis conditions (such as temperature, heating rate) and their impact on the yield of bio-oil obtained from pine needles have been studied (Varmal *et al*. 2015, 2018). These studies aim to optimize the process parameters to maximize the bio-oil yield and improve its quality. Catalysts can enhance the pyrolysis process by promoting specific reactions and improving the yield and quality of the resulting bio-oil. The effects of catalysts on the pyrolysis kinetic parameters of pine needles and the composition of bio-oil were explored (Gupta and Mondal 2021). The pyrolytic gases can contribute to the combustion process and energy generation when pine needles are burned. Researching the pyrolysis characteristics of pine needles, analyzing the composition of pyrolysis products, and exploring ways to enhance the production of pyrolysis gases will contribute to achieving complete combustion of pine needles. The distribution and composition of the products obtained from pyrolysis depend on various factors, such as temperature, heating rate, residence time, biomass feedstock, and pyrolysis process conditions. Optimization of these parameters can help tailor the pyrolysis process to maximize the desired product yields or specific properties of the products, such as higher gas production.

The pyrolysis of biomass is a complex process involving various thermochemical reactions such as char formation, fragmentation, depolymerization, and secondary mechanisms (Collard and Blin 2014). The evaluation of kinetic parameters is essential for understanding and predicting the dynamic conversion of biomass (Wang *et al*. 2017). Thermogravimetric analysis (TGA) is a commonly used method for characterizing the pyrolysis process and kinetics of various feedstocks (Tang *et al*. 2020; Ding *et al*. 2022).

The integration of kinetic and thermodynamic analyses using TG data is vital for estimating activation energy, designing and managing pyrolysis processes, acquiring pyrolytic byproducts, and facilitating scale-up for industrial applications. Monitoring the evolved products from PN pyrolysis can be effectively achieved by combining thermogravimetric analysis (TGA) with thermogravimetric analysis coupled with Fourier transform infrared spectroscopy (TG-FTIR) (Mehmood *et al*. 2019; Huang *et al*. 2020). Pyrolysis-gas chromatography/mass spectrometry (Py-GC/MS) is a technique commonly used to quantitatively investigate the product distribution from biomass pyrolysis with NIST library (Li *et al.* 2021; Nardella *et al.* 2022). In turn, this can provide insights for optimizing the distribution of pyrolysis products to enhance combustion efficiency.

In the present study, the thermogravimetric analysis of PN at the three heating rates (10, 20, and 40 °C/min) was carried out, and the kinetic and thermodynamic parameters were estimated. The pyrolysis mechanism of three components of PN (hemicellulose, cellulose, and lignin) was studied. The gas emissions and pyrolytic products were

determined by TG-FTIR and Py-GC/MS. The results provide guidance for the effective utilization of PN.

EXPERIMENTAL

Sample Pretreatment

The PN sample used in this study was collected from the countryside of Nanyang in Henan province of China. The samples were crushed and screened through 80-mesh sieve, after which they were dried at 80 °C for 24 h to remove moisture.

TG Experiments

The thermogravimetric experiment was conducted using an SDT Q600 TG analyzer from America, under a N_2 atmosphere. Samples weighing approximately 8.0 ± 0.5 mg were placed in Al_2O_3 crucibles. The TG experiments were heated from room temperature to 900 °C at heating rates of 10, 20, and 40 °C/min, with a nitrogen gas flow rate of 100 mL/min.

Reaction Kinetics of Pyrolysis

The TG results can be used to calculate kinetic parameters of biomass (Siddiqi *et al*. 2020). The pyrolysis reactions can be expressed as Eq. 1,

$$\alpha = \frac{m_0 - m_t}{m_0 - m_\infty} \quad (1)$$

where α is the conversion degree at time t (s), m_0 is the mass of initial time, m_t is the real-time mass at time *t*, and m_∞ is the remaining mass at the maximum pyrolysis temperature. The rate of mass change can be expressed as Eq. 2,

$$\frac{\mathrm{d}\alpha}{\mathrm{d}t} = kf(\alpha) \quad (2)$$

where $f(\alpha)$ is the conversion function which can be defined as Eq. 3:

$$f(\alpha) = (1-\alpha)^n \quad (3)$$

The PN pyrolysis was assumed to follow the first-order reaction model, where $n = 1$. In Eq. 2, k is the reaction constant, which can be expressed as Eq. 4,

$$K = A\exp(-E_a / RT) \quad (4)$$

where A is the pre-exponential factor, E_a denotes the activation energy, R is the universal gas constant (8.31 J/(K·mol)), and T is the reaction temperature (°C).

The heating rate is constant and defined as Eq. (5):

$$\beta = dT/dt \quad (5)$$

By combining equations 1, 3, 4, and 5, Eq. 6 can be obtained:

$$\frac{d\alpha}{\mathrm{d}T} = \frac{A}{\beta}\exp\left(-\frac{E_a}{RT}\right) f(a) \quad (6)$$

The integral function of conversion rate is assumed as $g(\alpha) = \int_0^\alpha d\alpha/f(\alpha)$, such that the equation can be expressed as follows (Eq. 7),

$$g(\alpha) = \int_0^\alpha d\alpha/f(\alpha) = (A/\beta)\int_{T_0}^T \exp(-E_a/RT)dT \quad (7)$$

In this study, the model-free methods of KAS and KWO method were adopted to estimate the E_a values of PN.

KAS method

KAS method was performed as shown by Kissinger *et al*. (1957) and Akahira and Sunose (1971). The key relationship can be expressed as Eq. 8,

$$\ln\frac{\beta}{T^2} = \ln(\frac{AE_a}{Rg(a)}) - \frac{E_a}{RT} \quad (8)$$

For a certain constant $g(a)$, the relationship between $\ln\frac{\beta}{T^2}$ and $1/T$ is a straight line. E_a was calculated with the line slope of $\frac{E_a}{R}$. *A* can be estimated by the line intercept.

FWO method

The FWO method is based on Doyle's approximation and the expression as following,

$$ln\,\beta = ln\frac{AE_\alpha}{Rg(\alpha)} - 5.335 - \frac{1.0516E_\alpha}{RT} \quad (9)$$

For a certain constant *g*(a), the line between $\ln\beta$ and $1/T$ is also a straight line. E_a is estimated with the slope expression $\left(-\frac{1.0516E_\alpha}{R}\right)$.

Kissinger - Kai method

The K-K method was developed from the Kissinger method (Kissinger *et al*. 1956; Li *et al*. 2014). The second derivative maxima of TG correspond to the peak locations for hemicellulose, cellulose and lignin, the expression as Eq. 10,

$$|\mathrm{DDTG}| = \left|\frac{d^2\left(\frac{m_t}{m_0}\right)}{dT^2}\right| = \left|\sum_{i=1}^{N} f_i \frac{d^2\alpha_i}{dT^2}\right| \geq 0 \quad (10)$$

where *N* is the total number of constituents ($\sum_{i=1}^{N} f_i = 1$)), f_i is the mass fraction of every constituent (i). As one constituent approaches the peak of reaction speed, the second derivative drops to a minimum. The activation energies for constituents are obtained as Eq. 11,

$$\ln\frac{\beta}{T_{p,i}^2} = \ln\left(\frac{AE_a}{Rg(a)}\right) - \frac{E_a}{RT_{p,i}} \quad (11)$$

where $T_{p,i}$ is the peak temperature of every constituent, the line between $\ln\frac{\beta}{T_{p,i}^2}$ and $\frac{1}{T_{p,i}}$ is plotted, and E_a of every component can be calculated from the slope expression.

TG–FTIR Experiments

Thermogravimetry (TGA 209 F3, Netzsch, Germany) together with a FTIR spectrometer (Bruker IFS 66/S, Bruker Optics, Billerica, MA) was used to analyze the evolved gases of PN pyrolysis. Samples of 8 ± 0.5 mg were placed in TG reactor and heated from room temperature to 900 °C with a rate of 10 °C/min, while the gas flow rate with the nitrogen was set as 70 mL/min. The temperature of the transmission line between TG and FTIR was set to 210 ℃ to prevent the produced gases condensation. The scanning resolution of FTIR was set to 8 cm^{-1} in the range of 600 to 4000 cm^{-1}, and data collection time of 60 min.

Py–GC/MS Experiments

A Py–GC/MS experiment was conducted to identify the pyrolysis volatiles using a Frontier pyrolyzer (EGA/PY-3030D, Japan) coupled to a GC/MS equipment (GCMS-QP 2010 Ultra, Shimadzu) equipped with a quartz capillary column (30 m × 0.25 mm × 0.25 μm). For each sample (0.10 mg), a vertical quartz tube was utilized, and silica wool was employed to prevent the escape of solid particles. Pyrolysis of the samples was performed at 600 °C for 10 seconds. The GC injector temperature was set to 250 °C, while the temperature of the chromatographic column was programmed as follows: (i) 50 °C for 5 minutes, (ii) ramping from 50 °C to 260 °C at a rate of 10 °C/min, and (iii) maintaining the temperature at 260 °C for 10 min. The carrier gas (helium) flow rate was set to 1.27 mL/min with a split ratio of 100:1. Mass spectra in total ion current mode were obtained within the mass range of m/z 35-500. The yield of the compounds was determined by referencing the NIST spectral libraries and relevant published literature.

RESULTS AND DISCUSSION

TG Curve Analysis

The DTG and TG curves of the PN are shown in Fig. 1. The tendency of TG/DTG curves are similar at different heating rates, which indicated that the same mechanism was active. Similar conclusions have been reported in many other studies (Gupta *et al*. 1957; Zou *et al*. 2010). Table 1 presents the pyrolysis parameters respectively.

Table 1. Pyrolysis Parameters of PN Composite

Heating Rate (°C/min)	T_{peak} (°C)	Mass Residue (%)
10	344	77.44
20	356	76.86
40	370	74.77

The peak temperatures of DTG at each heating rate were 344, 356, and 370 °C, respectively, shown in Fig. 1(a). The varied peak temperature was caused by thermal hysteresis. Biomass is a poor heat conductor, which leads to low heat transfer efficiency. The atmosphere temperature in TG analyzer heats up quickly with the high heating rate, and the time interval that the heat transferred to the sample center is longer, which caused the peak temperature at high heating rate to be larger, whereas a lower heating rate resulted in a uniform temperature of biomass (Loy *et al*. 2018).

Figure 1(b) shows that the main reaction occurred between 200 °C and 450 °C. This temperature range encompasses the pyrolysis of hemicellulose, cellulose, and lignin, which are the major components of biomass. The mass residue decreased with the increase of the heating rate as shown in Table 1. The lower residual mass with higher heating rate most likely resulted from the adequate decomposition of the reactants under the high heating rate. The average final residue was 77.4%.

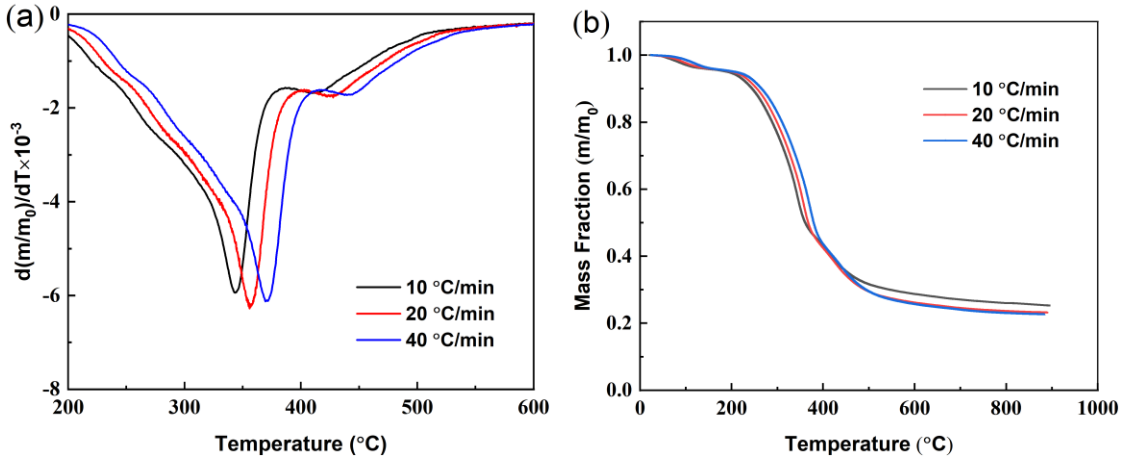

Fig. 1. (a) DTG curves, (b) TG curves

Dynamic Parameter of Thermal Decomposition

The dynamic parameters of thermal decomposition can be calculated from thermogravimetric data, such as activation energy (E_a) and pre-exponential factors (A). The KAS, FWO, and K-K methods described in the Experimental section were applied to calculate the activation energy of PN and the three main constituents (hemicellulose, cellulose, and lignin).

Activation energy of PN

The conversion rate from 0.1 to 0.9 was selected to calculate the activation energy of PN at different heating rates (10, 20, and 40 ℃ /min) based on the KAS and FWO methods. As described in the Experimental section, the KAS method plots ln (β/T^2) against $1/T$, which was shown in Fig. 2, and the FWO method plots $\ln\beta$ against $1/T$, as plotted in Fig. 3. The activation energy for varied conversion rates were calculated with the slopes ($(-E_a/R)$ of KAS and $\left(-\frac{1.0516E_\alpha}{R}\right)$ of FWO). The reaction order (n) was assumed to be one, and the reaction mechanism functions were calculated as $f(\alpha) = 1 - a$, and $g(a) = -\ln(1-a)$. On this basis, the pre-exponential factors were also determined.

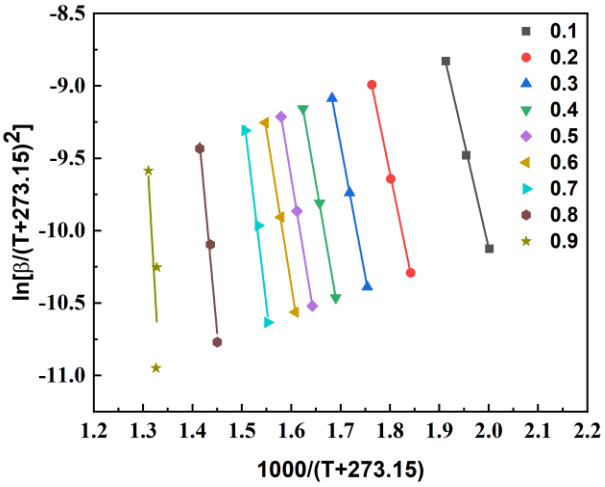

Fig. 2. KAS diagram of PN at varied conversion rates

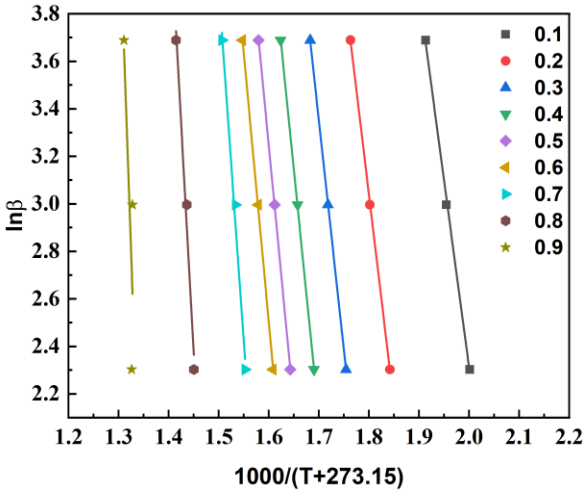

Fig. 3. FWO diagram of PN at varied conversion rates

Activation energies, pre-exponential factors, and coefficients of determination (R^2) of PN pyrolysis are listed in Table 2. The R^2 values were high, which indicated that the results were well suitable for the model equations.

The E_a increases with conversion rate, which denotes the decomposition of main biomass constituents. At the $0.1 < \alpha < 0.4$ stage, the activation energy range is 122 to 163 KJ/mol; this phase is mainly the hemicellulose pyrolysis stage. Decomposition takes place mainly by dehydration, decarboxylation, and the generation of small gas molecules such as decarburization and condensable volatiles, including breakage of C-O-C and C-C bonds and rupture of small molecule chains (Gangil and Bhargav 2018), which is consistent with thermogravimetric analysis. At the 0.5 to 0.7 stage, the activation energy ranged from 171 to 236 KJ/mol. This stage is mainly the pyrolysis stage of cellulose. Cellulose is a linear macromolecular polysaccharide composed of D-glucose group, which has high cohesion and hydrolysis resistance, and its degree of polymerization is higher than that of hemicelluloses (Gangil 2014). Lignin is a polymer containing an aromatic substrate that is involved in the crosslinking of hemicellulose and cellulose and thus is involved throughout the pyrolysis process. At the 0.8 to 0.9 stage, there is mainly a three-component carbonization process. The aromatic ring monomers produced by lignin depolymerization at this stage are more stable, so the activation energy is higher at this stage (Gupta *et al*. 2020).

The variation of E_a indicates that there are multi-step kinetics in the pyrolysis process, and the reason for the varied activation energy is that the chemical reactions of hemicellulose, cellulose, and lignin take place mainly at different temperatures. So hemicellulose, cellulose, and lignin in PN have different activation energies.

Activation energy of main components

The degradation sequence of those main components is hemicellulose, cellulose, and lignin with required activation energy (Grønli *et al*. 2002). The peak temperatures of them at varied heating rates are listed in Table 3, and the |DTG| and |DDTG| curves at heating rate 10 °C/min are shown in Fig. 4.

Table 2. E_a and A by KAS and FWO

α	KAS			FWO		
	E_a (kJ/mol)	R^2	ln$A$ (s^{-1})	E_a (kJ/mol)	R^2	ln$A$ (s^{-1})
0.10	122.38	0.99	7.49	124.45	0.99	27.28
0.20	137.27	0.99	8.92	139.31	0.99	28.88
0.30	150.92	0.99	10.63	152.72	0.99	30.69
0.40	163.29	0.99	12.19	164.82	0.99	32.32
0.50	171.35	0.99	13.06	172.75	0.99	33.25
0.60	177.28	0.99	13.70	178.61	0.99	33.94
0.70	235.53	0.99	23.35	234.32	0.99	43.65
0.80	307.55	0.98	32.92	303.51	0.98	53.36
0.90	-------	0.66	-------	-------	0.67	------
Mean	183.20		15.28	183.81		35.42

Table 3. The Peak Temperature of Main Components at Different Heating Rates and Activation Energy

T_{peak} (°C)	Heating Rate (°C /min)			Activation Energy (kJ/mol)
	10	20	40	
Hemicellulose	286	344	411	162
Cellulose	298	356	424	165
Lignin	306	370	439	184

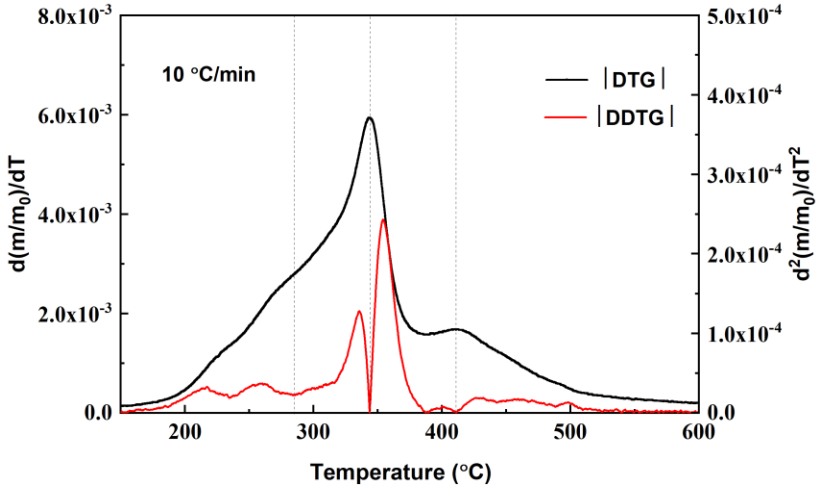

Fig. 4. Estimation of the peak locations based on |DTG| and |DDTG| at 10 °C/min

The activation energy of each component was calculated with K-K method. Figure 5 shows the relationship of $\frac{1}{T_{p,i}}$ virus $\ln\frac{\beta}{T_{p,i}^2}$. As can be seen in Table 3, the pyrolysis activation energy of the three components is in the order: lignin (184 kJ/mol) > cellulose (165 kJ/mol) > hemicellulose (162 kJ/mol). The trend was according to the activation energy of PN at varied conversion rates calculated in Table 2. Different inherent chemical structures and compositions may be caused by the varied activation energy of the main components. Hemicellulose is an amorphous structure composed of short chains with weak bonds, which is easily decomposed. Cellulose is a crystalline structure with a linear homopolysaccharide, which can be resistant to degradation. Lignin is a tridimensional

structure with a basic structure unit of phenylpropane. The higher energy requirement for lignin pyrolysis is primarily attributed to its intricate and interconnected structure (Chen *et al*. 2022).

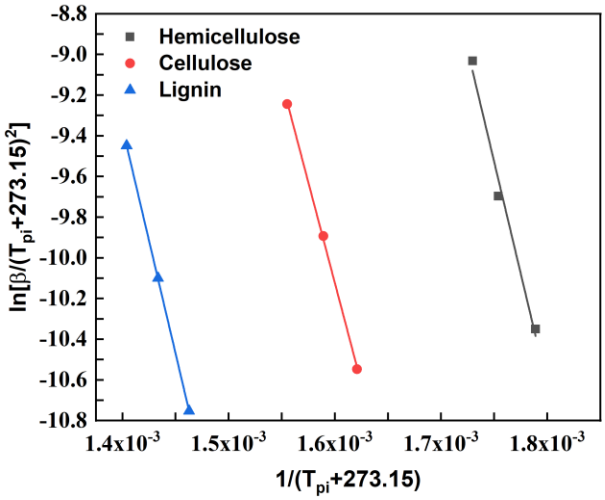

Fig. 5. K-K diagram of three components of PN

TG-FTIR analysis

Figure 6 shows three-dimensional infrared spectrum of the pyrolysis volatiles of PN at 10 ℃/min, which presents the absorbance as a function of wave number and temperature, and the release characteristics of the volatile gas are basically consistent with the DTG curves.

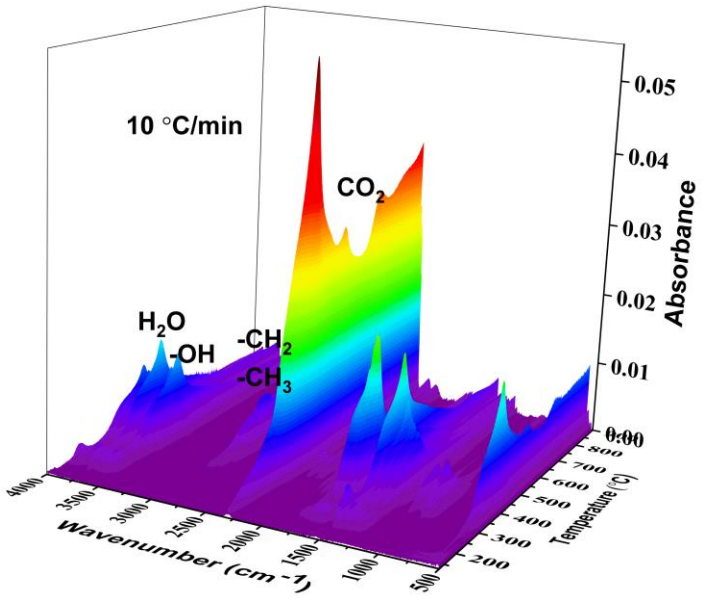

Fig. 6. Three-dimensional infrared spectra of PN

The composition of the pyrolysis volatiles can be determined from the characteristic peaks of infrared spectrum and the release sequence of the products can be estimated from absorption spectrum (Ma *et al*. 2018). As can be seen from Fig. 4, the peak temperature during pyrolysis process of PN is 344 °C at 10 ℃/min, and the absorption spectra curve at peak temperature is shown in Fig. 7.

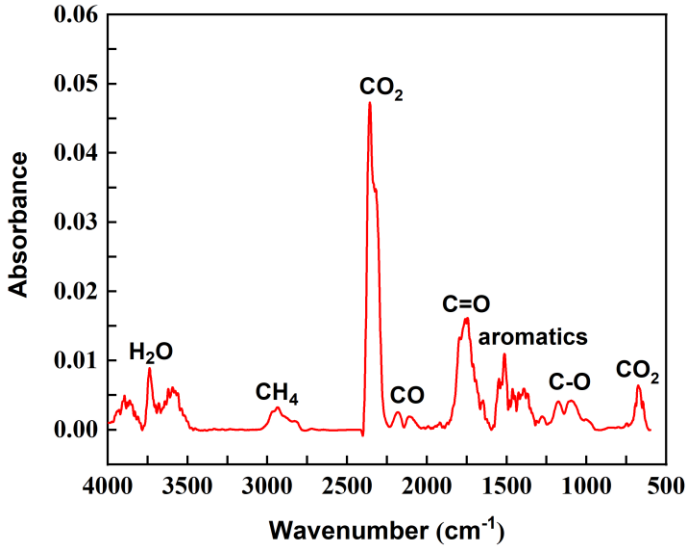

Fig. 7. TG-FTIR spectra of gas emissions at the peak temperature

The absorbance bands around 3500-4000 cm^{-1} showed the stretching vibration of hydroxyl (-OH) in H_2O. The presence of the fingerprint region 1400-1300 cm^{-1} represents the stretching vibration of hydroxyl group (-OH) in alcohol and phenol. The characteristic band ranged from 3000 to 2800 cm^{-1} and is related to C–H in methyl and methylene groups and produced CH_4. The absorption peak band of 2400-2240 cm^{-1} is caused by C=O in carbon dioxide, and there is a bending vibration of 660-680 cm^{-1} of carbon dioxide in the fingerprint region. The absorption peak band of 2240-2030 cm^{-1} represents CO emission. The characteristic band around 1850-1600 cm^{-1} represents C=O containing compounds (such as acids, aldehydes, and ketones). The 1600-1450 cm^{-1} was generated by C=C stretching vibration in benzene rings. The absorption peak around 1400-1050 cm^{-1} indicates compounds containing C–O, corresponding to the presence of phenols and alcohols, while absorptions around 1380 cm^{-1} was assigned to C–H. The main detected pyrolysis volatiles and functional groups were H_2O, CH_4, CO_2, CO, C=O, C=C, and C-O, which are listed in Table 4.

Table 4. Functional Groups and Gas Products of PN Pyrolysis by TG-FTIR

Functional Groups	Gas Products	Wavenumber Range
O-H	H_2O	4000-3500
(-CH_3, -CH_2)	CH_4	3000-2800, 1380
C=O	CO_2	2400-2240, 680-660
Carbonyl group (C=O)	Acids, aldehydes, ketones	1850-1600
C-O	CO	2240-2030
C-O	Alcohols, phenols	1400-1050
C=C	Aromatics	1550-1450
Hydroxyl group (-OH)	Alcohols, phenols, acids	4000-3500, 1400-1300

According to Lambert-Beer's Law, the absorption intensity of a specific compound becomes stronger in linear proportion as its concentration increases (Liu *et al.* 2008). Figure 8 presents the profiles of detected gas as the temperature increases during PN pyrolysis at a rate of 10 °C/min. Among the gases released from PN pyrolysis, the highest

amount was recorded for CO_2, followed by aromatic compounds and carbonyl compounds. On the other hand, CO emission was the lowest among the evolved gases. The peak temperature observed during the pyrolysis process of PN was 344 °C at a rate of 10 °C/min, which aligns with the findings from the TG experiment depicted in Fig. 4.

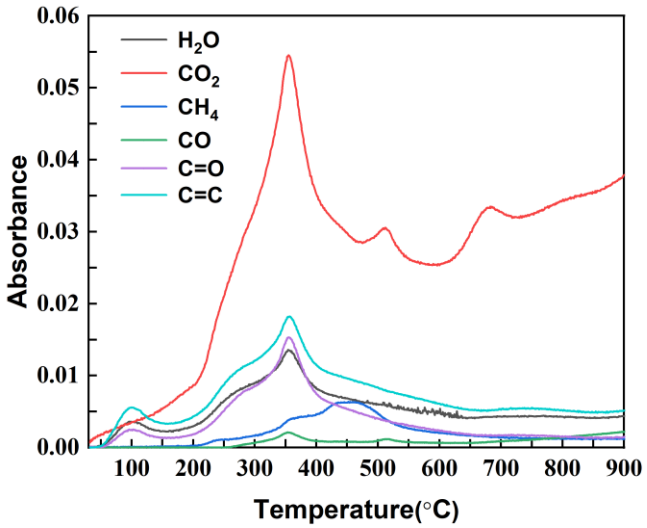

Fig. 8. Peak wavelengths profiles of PN pyrolysis products at 10 °C/min

Py-GC/MS Patterns

The pyrolysis temperature plays a crucial role in determining the type and yield of product compounds (Sun *et al*. 2020). In this study, based on Fig. 1, it was observed that the main components of PN were mostly degraded at 600 °C. Therefore, 600°C was selected as the fast pyrolysis temperature for the Py-GC/MS. The fast pyrolysis vapor of PN consists of non-condensable gases (such as CH_4, H_2, CO_2, CO, *etc*.) and volatile products. The volatile compounds undergo condensation to form liquid bio-oil, which was identified using the NIST database. The yield of different substances was estimated based on the relative peak area of each compound (Lu *et al*. 2011; Liu *et al*. 2021). Table 5 presents the main by-products of PN pyrolysis, as identified by Py-GC/MS. A total of 73 compounds were identified.

Table 5. Main By-products of the PN Pyrolysis Identified *via* Py-GC/MS

No.	Name of compound	Molecular formula	*m/z*	Group	RT (min)	Area (%)
1	Carbon dioxide	CO_2	44		1.450	2.86
Ketones						
2	Acetone	C_3H_6O	58	Ketones	1.655	5.36
3	2,3-Butanedione	$C_4H_6O_2$	86	Ketones	1.910	4.85
4	3-methyl-2-Pentanone	$C_6H_{12}O$	100	Ketones	1.965	1.99
5	2-Cyclopenten-1-one	C_5H_6O	82	Ketones	5.480	0.88
6	1-(acetyloxy)-2-Propanone	$C_5H_8O_3$	116	Ketones	6.520	0.55
7	4-Hydroxy-3-methylacetophenone	$C_9H_{10}O_2$	150	Ketones	15.530	0.91
8	Oxacyclotetradecan-2-one	$C_{13}H_{24}O_2$	212	Ketones	23.435	1.02
Hydrocarbons						
9	(Z)-1,3-Pentadiene	C_5H_8	68	Hydrocarbons	1.690	9.06
10	1,3-Cyclopentadiene	C_5H_6	66	Hydrocarbons	1.765	2.09
11	(Z)-3-Methyl-2-pentene	C_6H_{12}	84	Hydrocarbons	1.845	1.45

12	2-methyl-2-Pentene	C_6H_{12}	84	Hydrocarbons	2.010	2.95
13	2-Ethyl-1-butene	C_6H_{12}	84	Hydrocarbons	2.075	1.26
14	methylenevinyl-Cyclopropane	C_6H_8	80	Hydrocarbons	2.210	1.68
15	1,4-Cyclohexadiene	C_6H_8	80	Hydrocarbons	2.240	0.90
16	1,3-Cyclohexadiene	C_6H_8	80	Hydrocarbons	2.455	2.78
17	Benzene	C_6H_6	78	Hydrocarbons	2.520	0.57
18	2,3-dimethyl-Pentane	C_7H_{16}	100	Hydrocarbons	2.625	1.40
19	Heptane	C_7H_{16}	100	Hydrocarbons	2.715	1.14
20	Trans-1,5-Heptadiene	C_7H_{12}	96	Hydrocarbons	3.010	0.68
21	Toluene	C_7H_8	92	Hydrocarbons	3.720	1.42
22	1,3-Cycloheptadiene	C_7H_{10}	94	Hydrocarbons	3.855	0.48
23	Ethylbenzene	C_8H_{10}	106	Hydrocarbons	6.215	0.62
24	1,3-dimethyl-Benzene	C_8H_{10}	106	Hydrocarbons	6.445	0.92
25	1-Nonene	C_9H_{18}	126	Hydrocarbons	7.045	1.25
26	1,2,3-trimethyl-Benzene	C_9H_{12}	120	Hydrocarbons	8.885	0.51
27	1-Decene	$C_{10}H_{20}$	140	Hydrocarbons	9.545	0.82
28	2-propenyl-Benzene	C_9H_{10}	118	Hydrocarbons	9.660	0.48
29	Decane	$C_{10}H_{22}$	142	Hydrocarbons	9.735	0.61
30	D-Limonene	$C_{10}H_{16}$	136	Hydrocarbons	10.410	2.16
31	Undecane	$C_{11}H_{24}$	156	Hydrocarbons	11.795	0.71
32	1-Dodecene	$C_{12}H_{24}$	168	Hydrocarbons	13.440	0.67
33	1-Tridecene	$C_{13}H_{26}$	182	Hydrocarbons	15.050	0.64
34	Tridecane	$C_{13}H_{28}$	184	Hydrocarbons	15.165	0.56
35	1-Pentadecene	$C_{15}H_{30}$	210	Hydrocarbons	16.520	0.77
36	Tetradecane	$C_{14}H_{30}$	198	Hydrocarbons	16.625	0.47
37	Octadecane	$C_{18}H_{38}$	254	Hydrocarbons	17.985	0.49
Phenols						
38	Phenol	C_6H_6O	94	Phenols	9.405	4.47
39	2-methyl-Phenol	C_7H_8O	108	Phenols	10.985	1.06
40	p-Cresol	C_7H_8O	108	Phenols	11.390	1.86
41	2-methoxy-Phenol	$C_7H_8O_2$	124	Phenols	11.685	1.29
42	2,6-dimethyl-Phenol	$C_8H_{10}O$	122	Phenols	12.765	0.53
43	4-ethyl-Phenol	$C_8H_{10}O$	122	Phenols	13.085	0.54
44	2,5-dimethyl-Phenol	$C_8H_{10}O$	122	Phenols	13.115	0.61
45	Catechol	$C_6H_6O_2$	110	Phenols	13.660	1.75
46	Hydroquinone	$C_6H_6O_2$	110	Phenols	14.860	0.56
47	4-methyl-1,2-Benzenediol	$C_7H_8O_2$	124	Phenols	15.130	0.62
48	Eugenol	$C_{10}H_{12}O_2$	164	Phenols	16.170	0.49
49	2-methoxy-4-(1-propenyl)-Phenol	$C_{10}H_{12}O_2$	164	Phenols	17.490	0.55
Alcohols						
50	1-hydroxy-2-Propanone	$C_3H_6O_2$	74	Alcohols	2.355	5.25
51	1-Tetradecanol	$C_{14}H_{30}O$	214	Alcohols	17.890	1.39
52	Acetoin	$C_4H_8O_2$	88	Alcohols	2.825	0.74
53	1-Cyclohexene-1-methanol	$C_3H_{12}O$	112	Alcohols	3.260	1.10
54	2-methyl-1-Pentanol	$C_6H_{14}O$	102	Alcohols	4.195	0.99
55	1-Undecanol	$C_{11}H_{24}O$	172	Alcohols	11.640	0.64
Furans						
56	2,5-dimethyl-Furan	C_6H_8O	96	Furans	2.780	0.58
57	2-methyl-Furan	C_5H_6O	82	Furans	3.425	0.49
58	2,4-Dimethylfuran	C_6H_8O	96	Furans	9.060	0.65
59	2,3-dihydro-Benzofuran	C_8H_8O	120	Furans	13.960	2.61
Aldehydes						
60	2-Butenal	C_4H_6O	70	Aldehydes	2.280	1.45
61	Succindialdehyde	$C_4H_6O_2$	86	Aldehydes	3.985	1.23
62	Furfural	$C_5H_4O_2$	96	Aldehydes	5.430	0.68

63	p-Dodecyloxybenzaldehyde	$C_{19}H_{30}O_2$	290	Aldehydes	13.570	0.76
Acids						
64	(acetyloxy)-Acetic acid	$C_5H_8O_2$	118	Acids	3.745	2.15
65	Erucic acid	$C_9H_{14}O_2$	338	Acids	23.295	0.61
66	n-Hexadecanoic acid	$C_{28}H_{45}ClO_2$	256	Acids	23.355	0.97
Ester						
67	1-Propen-2-ol, acetate	$C_5H_8O_2$	100	Ester	1.810	0.76
68	Acrylic acid, cyclohexyl ester	$C_9H_{14}O_2$	154	Ester	2.580	1.09
69	Cholest-5-en-3-ol (3.beta.)-, carbonochloridate	$C_{28}H_{45}ClO_2$	448	Ester	32.845	1.03
70	Anisole	C_7H_8O	108	Ethers	7.765	0.52
Nitrides						
71	2-nitro-Propane	$C_3H_7NO_2$	89	Nitrides	3.100	0.53
72	Pyrrole	C_4H_5N	67	Nitrides	3.500	0.92
73	Indole	C_8H_7N	117	Nitrides	15.265	0.57

Figure 9 illustrates that the present bio-oil primarily consisted of olefin and aromatic hydrocarbons, phenols, alcohols, ketones, furans, nitrogenous compounds, and acids. These by-products have potential applications as fuels or raw chemicals (Chen *et al.* 2015; Mishra and Mohanty 2018). Decarboxylation reaction is responsible for the mass formation of hydrocarbons and the low amounts of acids (39.54% and 3.73%, respectively). The decarboxylation reaction possibly enhanced production of carbonyl compounds such as ketones and aldehydes (15.56% and 4.12%, respectively) (Gautam and Vinu 2018; Mishra *et al.* 2020). Additionally, the formation of alcohols facilitates further conversion into various hydrocarbons.

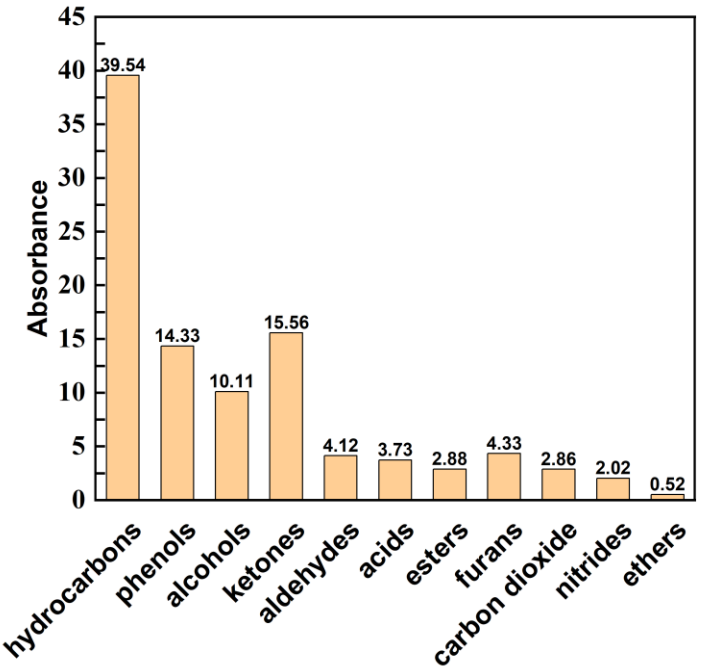

Fig. 9. Type and yield distributions of organic compounds from PN

Due to the deconstruction of lignin, high amounts of phenol were produced (14.3%) (Lu *et al.* 2018). The percentage of esters was low at 600 °C due to the formation of water molecules (Duprez *et al.* 1988). At a higher temperature (600 °C), carbon dioxide reacts

with char to produce carbon monoxide and induced the low amount of yield (2.86%), which was also proved by TG-FTIR. N-containing compounds (2-nitro-propane, pyrrole, and indole) were formed by the deamination reaction from the decomposition of proteins and carbohydrates present in biomass (Setter *et al*. 2019). The furans were produced from the dehydration reactions of cellulose and hemicelluloses (Hidayat *et al*. 2018).

CONCLUSIONS

.

1. The pyrolysis behavior and kinetics of pine needles (PN) were investigated using thermogravimetry-Fourier transform infrared (TG-FTIR) and pyrolysis-gas chromatography/mass spectrometry (Py-GC/MS). The kinetic analysis of PN confirmed the variation in activation energy during the progressive conversion. The peak pyrolysis temperature of pine PN ranged from 344 to 370 °C at different heating rates.
2. The mean activation energies of PN were calculated using the KAS and FWO methods, resulting in values of 183.2 and 183.8 kJ/mol, respectively. The K-K method was employed to calculate the activation energy of the main components, highlighting the higher energy requirement for lignin pyrolysis due to its intricate and interconnected structure.
3. TG-FTIR analysis revealed the presence of pyrolysis volatiles, including CO_2, H_2O, CO, CH_4, phenols, and other gases. Py-GC/MS analysis indicated that hydrocarbons, phenols, alcohols, ketones, and aldehydes were the main decomposition products.
4. Kinetic parameters provide fundamental information for predicting the rates at which chemical reactions occur. By incorporating these parameters into reactor design models, engineers can accurately estimate reaction rates and optimize reactor performance. Studying pyrolysis behavior and understanding the composition of the pyrolysis gas from pine needles can provide valuable information for achieving complete combustion.

ACKNOWLEDGMENTS

This study is supported by International Science and Technology Cooperation Project of Henan Province (232102521011); Key Research and Development and Promotion Project in Henan province-Science and Technology (International Cooperation) (182102410087, 222102520016); Henan International Joint Laboratory of Thermo-fluid Electro-chemical System for New Energy Vehicle; Key R & D Plan of Sichuan Science and Technology Program (2022YFG0138); Agricultural Science and Technology Innovation Project of Chinese Academy of Agricultural Sciences (CAAS-ASTIP-2016-BIOMA).

REFERENCES CITED

Akahira, T., and Sunuse, T. T. (1971). "Joint convention of four electrical institutes," *Report of Research, Chiba Institute of Technology.* 16, 22-31.

Chen, L., Wang, X., Yang, H., Lu, Q., Li, D., Yang, Q., and Chen, H. (2015). "Study on pyrolysis behaviors of non-woody lignins with TG-FTIR and Py-GC/MS," *Journal of Analytical and Applied Pyrolysis* 113, 499-507. DOI: 10.1016/j.jaap.2015.03.018

Chen, D., Cen, K., Zhuang, X., Gan, Z., Zhou, J., Zhang, Y., and Zhang, H. (2022). "Insight into biomass pyrolysis mechanism based on cellulose, hemicellulose, and lignin: Evolution of volatiles and kinetics, elucidation of reaction pathways, and characterization of gas, biochar and bio-oil," *Combustion and Flame* 242, article 112142. DOI: 10.1016/j.combustflame.2022.112142

Collard, F. X., and Blin, J. (2014). "A review on pyrolysis of biomass constituents: Mechanisms and composition of the products obtained from the conversion of cellulose, hemicelluloses and lignin," *Renewable and Sustainable Energy Reviews* 38, 594-608. DOI: 10.1016/j.rser.2014.06.013

Dhyani, V., and Bhaskar, T. (2018). "A comprehensive review on the pyrolysis of lignocellulosic biomass," *Renewable Energy* 129, 695-716. DOI: 10.1016/j.renene.2017.04.035

Ding, Y., Huang, B., Li, K., Du, W., Lu, K., and Zhang, Y. (2020). "Thermal interaction analysis of isolated hemicellulose and cellulose by kinetic parameters during biomass pyrolysis," *Energy* 195, article 117010. DOI: 10.1016/j.energy.2020.117010

Ding, Y., Zhang, W., Zhang, X., Han, D., Liu, W., and Jia, J. (2022). "Pyrolysis and combustion behavior study of PMMA waste from microscale to bench-scale experiments," *Fuel* 319, article 123717. DOI: 10.1016/j.fuel.2022.123717

Duprez, D., Barrault, J., and Geron, C. (1988). "Effect of partial reduction on the formation of oxygenated compounds in the hydrogenation of carbon monoxide on rhodium/alumina," *Applied Catalysis* 37, 105-114. DOI: 10.1016/S0166-9834(00)80754-X

Fu, J., Liu, J., Xu, W., Chen, Z., Evrendilek, F., and Sun, S. (2022). "Torrefaction, temperature, and heating rate dependencies of pyrolysis of coffee grounds: Its performances, bio-oils, and emissions," *Bioresource Technology* 345, article 126346. DOI: 10.1016/j.biortech.2021.126346

Gangil, S., and Bhargav, V. K. (2018). "Influence of torrefaction on intrinsic bioconstituents of cotton stalk: TG-insights," *Energy* 142, 1066-1073. DOI: 10.1016/j.energy.2017.10.128

Gangil, S. (2014). "Distinct splitting of polymeric cellulosic signals in cashew shell: A TG-diagnosis," *Cellulose* 21, 2913-2924. DOI: 10.1007/s10570-014-0309-0

Gautam, R., and Vinu, R. (2018). "Non-catalytic fast pyrolysis and catalytic fast pyrolysis of *Nannochloropsis oculata* using Co-Mo/γ-Al_2O_3 catalyst for valuable chemicals," *Algal Research* 34, 12-24. DOI: 10.1016/j.algal.2018.06.024

Grønli, M., Várhegyi, G., and Blasi, C. D. (2002). "Thermogravimetric analysis and devolatilization kinetics of wood," *Industrial & Engineering Chemistry Research* 41, 4201-4208. DOI: 10.1021/ie0201157

Gupta, S., Gupta, G. K., and Mondal, M. K. (2019). "Slow pyrolysis of chemically treated walnut shell for valuable products: Effect of process parameters and in-depth product analysis," *Energy* 181, 665-676. DOI: 10.1016/j.energy.2019.05.214

Gupta, G. K., and Mondal, M. K. (2019). "Kinetics and thermodynamic analysis of maize cob pyrolysis for its bioenergy potential using thermogravimetric analyzer," *Journal of Thermal Analysis and Calorimetry* 137, 1431-1441. DOI: 10.1007/s10973-019-08053-7

Gupta, S., and Mondal, P. (2021). "Catalytic pyrolysis of pine needles with nickel doped gamma-alumina: Reaction kinetics, mechanism, thermodynamics and products analysis," *Journal of Cleaner Production* 286, article 124930. DOI: 10.1016/j.jclepro.2020.124930

Gupta, S., Patel, P., and Mondal, P. (2022). "Biofuels production from pine needles *via* pyrolysis: Process parameters modeling and optimization through combined RSM and ANN based approach," *Fuel* 310, article 122230. DOI: 10.1016/j.fuel.2021.122230

Gupta, S., and Mondal, P. (2021). "Catalytic pyrolysis of pine needles with nickel doped gamma-alumina: Reaction kinetics, mechanism, thermodynamics and products analysis," *Journal of Cleaner Production* 286, article 124930. DOI: 10.1016/j.jclepro.2020.124930

Hidayat, S., Bakar, M. S. A., Yang, Y., Phusunti, N., and Bridgwater, A. V. (2018). "Characterisation and Py-GC/MS analysis of *Imperata cylindrica* as potential biomass for bio-oil production in Brunei Darussalam," *Journal of Analytical and Applied Pyrolysis* 134, 510-519. DOI: 10.1016/j.jaap.2018.07.018

Huang, H., Liu, J., Liu, H., Evrendilek, F., and Buyukada, M. (2020). "Pyrolysis of water hyacinth biomass parts: Bioenergy, gas emissions, and by-products using TG-FTIR and Py-GC/MS analyses," *Energy Conversion and Management* 207, article 112552. DOI: 10.1016/j.enconman.2020.112552

Huang, R., Huang, Z., Ran, Y., Xiong, X., Luo, T., Long, E., Mei, Z., and Wang, J. (2021). "Experimental and simulation study on the surface contact between biogas fermentation liquid and straw material based on hydraulic mixing," *Energy* 222, article 119992. DOI: 10.1016/j.energy.2021.119992

Kissinger, H. E. (1956). "Variation of peak temperature with heating rate in differential thermal analysis," *Journal of Research of the National Bureau of Standards* 57(4), 217-221.

Kissinger, H. E. (1957). "Reaction kinetics in differential thermal analysis," *Analytical Chemistry* 29, 1702-1706. DOI: 10.1021/ac60131a045

Li, K. Y., Huang, X., Fleischmann, C., Rein, G., and Ji, J. (2014). "Pyrolysis of medium-density fiberboard: Optimized search for kinetics scheme and parameters *via* a genetic algorithm driven by Kissinger's method," *Energy Fuels* 28(9), 6130-6139. DOI: 10.1021/ef501380c

Li, J., Dou, B., Zhang, H., Zhang, H., Chen, H., Xu, Y., and Wu, C. (2021). "Pyrolysis characteristics and non-isothermal kinetics of waste wood biomass," *Energy* 226, article 120358. DOI: 10.1016/j.energy.2021.120358

Liu, Q., Wang, S., Zheng, Y., Luo, Z., and Cen, K. (2008). "Mechanism study of wood lignin pyrolysis by using TG–FTIR analysis," *Journal of Analytical and Applied Pyrolysis* 82, 170-177. DOI: 10.1016/j.jaap.2008.03.007

Liu, H., Liu, J., Huang, H., Evrendilek, F., Wen, S., and Li, W. (2021). "Optimizing bioenergy and by-product outputs from durian shell pyrolysis," *Renewable Energy* 164, 407-418. DOI: 10.1016/j.renene.2020.09.044

Loy, A. C. M., Gan, D. K. W., Yusup, S., Chin, B. L. F., Lam, M. K., Shahbaz, M., Unrean, P., Acda, M. N., and Rianawati, E. (2018). "Thermogravimetric kinetic

modelling of insitu catalytic pyrolytic conversion of rice husk to bioenergy using rice hull ash catalyst," *Bioresource Technology* 261, 213-222. DOI: 10.1016/j.biortech.2018.04.020

Lu, Q., Yang, X., Dong, C., Zhang, Z., Zhang, X., and Zhu X. (2011). "Influence of pyrolysis temperature and time on the cellulose fast pyrolysis products: Analytical Py-GC/MS study," *Journal of Analytical and Applied Pyrolysis* 92, 430-438. DOI: 10.1016/j.jaap.2011.08.006

Lu, Q., Guo, H., Zhou, M., Zhang, Z., Cui, M., Zhang, Y., Yang, Y., and Zhang, L. (2018). "Monocyclic aromatic hydrocarbons production from catalytic cracking of pine wood-derived pyrolytic vapors over Ce-Mo2N/HZSM-5 catalyst," *Science of the Total Environment* 634, 141-149. DOI: 10.1016/j.scitotenv.2018.03.351

Ma, Z., Wang, J., Yang, Y., Zhang, Y., Zhao, C., Yu, Y., and Wang, S. (2018). "Comparison of the thermal degradation behaviors and kinetics of palm oil waste under nitrogen and air atmosphere in TGA-FTIR with a complementary use of model-free and model-fitting approaches," *Journal of Analytical and Applied Pyrolysis* 134, 12-24. DOI: 10.1016/j.jaap.2018.04.002

Mehmood, M. A., Ahmad, M. S., Liu, Q., Liu, C. G., Tahir, M. H., Aloqbi, A. A., Tarbiah, N. I., Alsufiani, H. M., and Gull, M. (2019). "*Helianthus tuberosus* as a promising feedstock for bioenergy and chemicals appraised through pyrolysis, kinetics, and TG-FTIR-MS based study," *Energy Conversion and Management* 194, 37-45. DOI: 10.1016/j.enconman.2019.04.076

Mishra, R. K., and Mohanty, K. (2018). "Thermocatalytic conversion of non-edible Neem seeds towards clean fuel and chemicals," *Journal of Analytical and Applied Pyrolysis* 134, 83-92. DOI: 10.1016/j.jaap.2018.05.013

Mishra, R.K., Mohanty, K., and Wang, X. (2020). "Pyrolysis kinetic behavior and Py-GC–MS analysis of waste dahlia flowers into renewable fuel and value-added chemicals," *Fuel* 260, article 116338. DOI: 10.1016/j.fuel.2019.116338

Nardella, F., Bellavia, S., Mattonai, M., and Ribechini, E. (2022). "Co-pyrolysis of biomass and plastic: Synergistic effects and estimation of elemental composition of pyrolysis oil by analytical pyrolysis–gas chromatography/mass spectrometry," *Bioresource Technology* 354, article 127170. DOI: 10.1016/j.biortech.2022.127170

Setter, C., Silva, F. T. M., Assis, M. R., Ataíde, C. H., Trugilho, P. F., and Oliveira, T. J. P. (2019). "Slow pyrolysis of coffee husk briquettes: Characterization of the solid and liquid fractions," *Fuel* 261, article 116420. DOI: 10.1016/j.fuel.2019.116420

Siddiqi, H., Bal, M., Kumari, U., and Meikapabc, B. C. (2020). "In-depth physiochemical characterization and detailed thermo-kinetic study of biomass wastes to analyze its energy potential," *Renewable Energy* 148, 756-771. DOI: 10.1016/j.renene.2019.10.162

Sun, Z., Xu, B., Rony, A. H., Toan, S., Chen, S., Gasem, K. A.M., Adidharma, H., Fan, M., and Xiang, W. (2017). "Thermogravimetric and kinetics investigation of pine wood pyrolysis catalyzed with alkali-treated CaO/ZSM-5," *Energy Conversion and Management* 146, 182-194. DOI: 10.1016/j.enconman.2017.04.104

Sun, T., Li, Z., Zhang, Z., Wang, Z., Yang, S., Yang, Y., Wang, X., Liu, S., Zhang, Q., and Lei, T. (2020). "Fast corn stalk pyrolysis and the influence of catalysts on product distribution," *Bioresource Technology* 301, article 122739. DOI: 10.1016/j.biortech.2020.122739

Tang, X., Chen, Z., Liu, J., Chen Z., Xie W., Evrendilek, F., and Buyukada, M. (2020). "Dynamic pyrolysis behaviors, products and mechanisms of waste rubber and

polyurethane bicycle tires," *Journal of Hazardous Materials* 402, article 123516. DOI: 10.1016/j.jhazmat.2020.123516

Varma, A. K., and Mondal, P. (2015). "Physicochemical characterization and kinetic study of pine needle for pyrolysis process," *Journal of Thermal Analysis and Calorimetry* 124, 487-497. DOI 10.1007/s10973-015-5126-7

Varma, A. K., and Mondal, P. (2018). "Pyrolysis of pine needles: Effects of process parameters on products yield and analysis of products," *Journal of Thermal Analysis and Calorimetry* 131, 2057-2072. DOI: 10.1007/s10973-017-6727-0

Wang, S., Dai, G., Yang, H., and Luo, Z. (2017). "Lignocellulosic biomass pyrolysis mechanism: A state-of-the-art review," *Progress in Energy & Combustion Science* 62, 33-86. DOI: 10.1016/j.pecs.2017.05.004

Wang, J., Xue, Q., Guo, T., Mei, Z., Long, E., Wen, Q., Huang, W., Luo, T., and Huang, R. (2018). "A review on CFD simulating method for biogas fermentation material fluid," *Renewable & Sustainable Energy Reviews* 97, 64-73. DOI: 10.1016/j.rser.2018.08.029

Wang, Z., Bui, Q., Zhang, B., and Phama, T. L. H. (2020). "Biomass energy production and its impacts on the ecological footprint: an investigation of the G7 countries," *Science of the Total Environment* 743, article 140741. DOI: 10.1016/j.scitotenv.2020.140741

Xu, L., Zhou, J., Ni, J., Li, Y., Long, Y., and Huang, R. (2020). "Investigating the pyrolysis kinetics of *Pinus sylvestris* using thermogravimetric analysis," *BioResources* 15(3), 5577-5592. DOI: 10.15376/biores.15.3.5577-5592

Yasmeen, R., Cui, Z., Shah, W. U. H., Kamal, M. A., and Khan, A. (2022). "Exploring the role of biomass energy consumption, ecological footprint through FDI and technological innovation in B&R economies: A simultaneous equation approach," *Energy* 244, article 122703. DOI: 10.1016/j.energy.2021.122703

Zou, S., Wu, Y., Yang, M., Li, C., and Tong, J. (2010). "Pyrolysis characteristics and kinetics of the marine microalgae *Dunaliella tertiolecta* using thermogravimetric analyzer," *Bioresource Technology* 101, 359-365. DOI: 10.1016/j.biortech.2009.08.020

Article submitted: June 11, 2023; Peer review completed: June 24, 2023; Revised version received: July 21, 2023; Accepted: July 22, 2023; Published: July 31, 2023.
DOI: 10.15376/biores.18.3.6412-6429